scientific reports

Check for updates

OPEN

Joint metabolomics and transcriptomics analysis systematically reveal the impact of *MYCN* in neuroblastoma

Bang Du[1], Yingyu Zhang[2], Pin Zhang[1], Mengxin Zhang[1], Zhidan Yu[1], Lifeng Li[1], Ligong Hou[3], Qionglin Wang[4]✉, Xianwei Zhang[1]✉ & Wancun Zhang[1,3,4]✉

The limited understanding of the molecular mechanism underlying *MYCN*-amplified (MNA) neuroblastoma (NB) has hindered the identification of effective therapeutic targets for MNA NB, contributing to its higher mortality rate compared to *MYCN* non-amplified (non-MNA) NB. Therefore, a comprehensive analysis integrating metabolomics and transcriptomics was conducted to systematically investigate the MNA NB. Metabolomics analysis utilized plasma samples from 28 MNA NB patients and 68 non-MNA NB patients, while transcriptomics analysis employed tissue samples from 15 MNA NB patients and 37 non-MNA NB patients. Notably, joint metabolomics and transcriptomics analysis was performed. A total of 46 metabolites exhibited alterations, with 21 displaying elevated levels and 25 demonstrating reduced levels in MNA NB. In addition, 884 mRNAs in MNA NB showed significant changes, among which 766 mRNAs were higher and 118 mRNAs were lower. Joint-pathway analysis revealed three aberrant pathways involving glycerolipid metabolism, purine metabolism, and lysine degradation. This study highlights the substantial differences in metabolomics and transcriptomics between MNA NB and non-MNA NB, identifying three abnormal metabolic pathways that may serve as potential targets for understanding the molecular mechanisms underlying MNA NB.

Keywords *MYCN* amplification, Neuroblastoma, Metabolomics, Transcriptomics, Therapeutic target, Molecular mechanism

Neuroblastoma (NB) is a malignancy of the peripheral nervous system that arises from the embryonic neural crest, characterized by an insidious onset and rapid progression. NB constitutes 8% of all pediatric cancer cases, while accounting for 15% of childhood[1–3]. The clinical manifestations of NB exhibit significant heterogeneity, ranging from spontaneous regression or differentiation with an overall survival rate of 85–90%, to refractory and metastatic tumors, wherein less than 50% of patients survive even after intensive therapy[4]. One of the factors contributing to NB heterogeneity is *MYCN* amplification (MNA), which has been shown to promote NB growth and progression, and correlate with treatment resistance and unfavorable prognosis in NB[5]. For instance, in comparison to MNA NB, *MYCN* non-amplified (non-MNA) NB patients had higher event free survival (EFS) and overall survival (OS) (EFS and OS: 82.5% and 90.8% versus 36.9% and 44.8%), indicating that MNA has a tremendous impact on the prognosis of NB[6]. Furthermore, the prevalence of MNA in NB patients is 20–30%, whereas MNA is detected in about 50% of high risk NB (HR-NB) cases with an overall survival rate of less than 50%[7,8]. Studies have also shown that *MYCN*, as a major transcription factor, is important for normal cell proliferation and apoptosis. MNA may lead to inhibition of apoptosis signals and continuous proliferation, which may eventually lead to the development of NB[9]. Nevertheless, there is a dearth of studies that explicitly elucidate the

[1]Health Commission of Henan Province Key Laboratory for Precision Diagnosis and Treatment of Pediatric Tumor, Children's Hospital Affiliated to Zhengzhou University, Zhengzhou 450018, China. [2]The First Affiliated Hospital, College of Clinical Medicine of Henan University of Science and Technology, Henan Key Laboratory of Rare Diseases, Endocrinology and Metabolism Center, Luoyang 471003, China. [3]Henan International Joint Laboratory for Prevention and Treatment of Pediatric Disease, Children's Hospital Affiliated to Zhengzhou University, Zhengzhou 450018, China. [4]Henan Key Laboratory of Children's Genetics and Metabolic Diseases, Children's Hospital Affiliated to Zhengzhou University, Zhengzhou 450018, China. ✉email: wangqionglin2020@163.com; zhangxw956658@126.com; zhangwancun@126.com

molecular mechanism underlying MNA in NB or its associated therapeutic targets, thereby contributing to the elevated mortality observed in MNA NB compared to non-MNA NB[10]. Therefore, it is imperative to investigate the aberrant pathway of MNA NB in order to elucidate the molecular regulatory mechanism underlying MNA in NB and subsequently identify potential therapeutic targets for augmenting the survival rate of patients with MNA NB.

It is worth noting that the development of omics has been expected to make important contributions to the understanding of *MYCN* molecular mechanisms and the discovery of therapeutic targets of MNA NB. Metabolomics aims to characterize all small molecules in a sample to accurately reflect the biological metabolic signature of the disease, which is beneficial to understanding the pathological or physiological conditions. The MNA exerts an impact on various metabolic pathways in NB, exemplified by the ability of *MYCN* to bind to the E-box within the promoter region of the p53 gene and enhance p53 transcription. Notably, there exists a positive correlation between p53 expression in NB tissue and *MYCN* expression[11]. Furthermore, *MYCN* can bind to the promoter region of ASCT2, a glutamine carrier, promoting its transcription. Enhanced glutamine metabolism represents a crucial characteristic of malignant tumors; thus, during proliferation processes, NB cells with amplified *MYCN* necessitate substantial amounts of glutamine for their proliferation support[12]. Consequently, it is imperative to further investigate the relationship between *MYCN* and tumor metabolism. It has been found that MNA NB is correlated with altered expression of proteins involved in multiple metabolic processes, including enhanced glycolysis and increased oxidative phosphorylation compared with non-MNA NB[13,14]. Konstantinos et al.[15] found that *MYCN* changed the sulfur transfer pathway in NB through metabolomics. Arlt et al.[16] found that phosphoglycerate dehydrogenase is related to MNA through metabolomics analysis, and MNA NB has higher synthesis of serine than non-MNA NB. In addition, through metabolomics analysis, Alptekin et al.[17] revealed that MNA affects purine and central carbon metabolism and reduces citrate production, leading to a decrease in the steady-state levels of cholesterol and fatty acids. Transcriptomics utilizes high-throughput sequencing techniques to investigate the comprehensive repertoire of transcribed mRNAs in specific cells, tissues, or individuals at a given temporal and physiological state. This approach enables the identification of disparities in gene expression and structure across distinct functional states, thereby facilitating the elucidation of molecular mechanisms underlying diverse pathological or physiological conditions[18,19]. Fan et al.[20] studied differential genes between MNA NB and non-MNA NB through transcriptomics and found that *FLVCR2*, *SCN7A*, *PRSS12*, *NTRK1* and *XAGE1A* could be used as biomarkers to predict the prognosis of MNA NB. Lee et al.[21] conducted transcriptome analysis on non-MNA NB, providing new insights into the genomic background of non-MNA NB. In addition, research had found that *EZH1* depletion in MNA NB cells resulted in significant cell death as well as xenograft inhibition[22]. With the rapid development of omics, multi-omics analysis has made important contributions to heart failure, colorectal cancer, bladder cancer and other diseases[23–25]. The integration of transcriptomics and metabolomics has been demonstrated as a robust methodology, which can enhance the comprehension of potential biological functions and molecular mechanisms underlying diseases[26]. Metabolomics and transcriptomics have been used to study the metabolomics and transcriptomics differences between MNA NB and non-MNA, respectively. However, a comprehensive integration of metabolomics and transcriptomics is noticeably lacking in the investigation of molecular mechanisms and therapeutic targets associated with MNA in NB. Therefore, the integration of metabolomics and transcriptomics holds immense significance in comprehending the molecular mechanisms influenced by MNA and facilitating the identification of therapeutic targets for MNA NB.

In this study, a total of 96 plasma clinical samples and 52 clinical NB tissue samples were subjected to metabolomics and transcriptomics analyses, respectively. The integration of metabolomics and transcriptomics data was employed to perform a comprehensive network analysis of MNA NB, elucidating molecular mechanisms and identifying potential therapeutic targets. The innovation of this study lies in the comprehensive analysis of the differences between MNA NB and non-MNA NBA through integrated metabolomics and transcriptomics analysis, aiming to elucidate the molecular mechanism underlying MNA and identify potential therapeutic targets. Furthermore, investigating aberrant metabolic pathways in MNA NB provides a theoretical foundation for understanding its molecular mechanisms and subsequent exploration of therapeutic targets.

Methods and materials

Sample collection

This study was granted approval by the Ethics Committee of Henan Children's Hospital (2019-H-K11), and all procedures were conducted in accordance with relevant guidelines and regulations. A total of 96 plasma samples (28 cases of MNA NB, 68 cases of non-MNA NB) and 52 NB tissue samples (15 cases of MNA NB, 37 cases of non-MNA NB) were collected and processed at the Henan Children's Hospital from October 2018 to January 2022. The plasma samples were taken from the fasting plasma of NB patients on the morning of surgery, and tissue samples were taken from tumor tissues of NB patients during surgery.

Some patients underwent tumor evaluation at our hospital but did not undergo surgery, resulting in the availability of only blood samples without corresponding NB tissue samples. Conversely, other patients were referred for surgical intervention after preoperative examinations at different facilities, yielding only tissue samples without accompanying blood samples. Consequently, a subset of patients provided both blood and tissue samples. To enhance the statistical power of our study and ensure more comprehensive results, we incorporated plasma and tissue samples from 41 children, solely tissue samples from an additional 11 children, and exclusively plasma samples from another 55 children. Patient information is illustrated using a Venn diagram in Fig. S1.

Inclusion criteria consisted of: (1) confirmed diagnosis of pathological NB; (2) the MNA status in NB tissue was clear; (3) informed consent was signed by children or their parents. Exclusion criteria consisted of: (1) complications of other diseases; (2) informed consent was not signed by children or their parents. Plasma samples were collected before the surgery and were immediately frozen at − 80 °C for metabolomics analyses. NB tissue

samples were directly placed into liquid nitrogen after surgical resection until transcriptomics analysis. Tables S1 and S2 showed that there were no significant differences in the age, male to female ratio, *MYCN* value and gross tumor volume between MNA NB and non-MNA NB patients. On the other hand, there were statistical differences in tumor metastasis, radiological risk factors and HR-NB (based on COG classification) ratio between MNA NB and non-MNA NB patients.

Metabolomics analysis via high performance liquid chromatography-mass spectrometry (HPLC–MS)

The metabolomics approach we employ is consistent with the methodology outlined in our previous publication[19]. The metabolomics analysis was performed using MetaboAnalyst (https://www.metaboanalyst.ca/MetaboAnalyst/home.xhtml), which included partial least-squares discrimination analysis (PLS-DA), heatmap, volcano map, enrichment analysis, pathway analysis, and identification of biomarkers. The stability of the overall experimental results was evaluated by preparing a quality control (QC) sample, which was obtained by combining equal volumes of supernatant from all samples.

Transcriptomics detection through RNA-sequencing (RNA-seq) analysis

Total RNA was extracted using TRIzol reagent according to the manufacturer's protocol. RNA purity and quantification were evaluated using the NanoDrop 2000 spectrophotometer (Thermo Scientific, USA). RNA integrity number (RIN) was assessed using the Agilent 2100 Bioanalyzer (Agilent Technologies, Santa Clara, CA, USA). The libraries were constructed using TruSeq Stranded mRNA LT Sample Prep Kit (Illumina, San Diego, CA, USA) according to the manufacturer's instructions. The transcriptome sequencing and analysis were conducted by OE Biotech Co., Ltd. (Shanghai, China). The libraries were sequenced on an Illumina HiSeq X Ten platform and 150 bp paired-end reads were generated. About 48.349 M raw reads for each sample were generated. Raw data (raw reads) of fastq format were firstly processed using Trimmomatic and the low quality reads were removed to obtain clean reads[27]. The clean reads were mapped to the human genome (GRCh38) using HISAT2[28]. Fragments per kilobase of exon model per million mapped fragments (FPKM) of each gene were calculated using Cufflinks and the read counts of each gene were obtained by HTSeq-count[29,30]. P value < 0.05 and $|\log_2(\text{fold change})| > 1$ were set as the threshold for significantly differential expression. Hierarchical cluster analysis of differentially expressed genes was performed to demonstrate the expression pattern of genes in different groups and samples. Open database sources, including the Gene Ontology (GO), Kyoto Encyclopedia of Genes and Genomes (KEGG)[31–33], MetaboAnalyst, Human Metabolome Database and National Center for Biotechnology Information (NCBI) were used to identify metabolic pathways.

Joint analysis of the metabolomics and transcriptomics

Finally, comprehensive transcriptomics and metabolomics analyses were conducted using MetaboAnalyst 5.0 to perform a joint-pathway analysis module for topological assessment of individual molecules (i.e., nodes) based on their position in the network. Official gene symbols and compound names, along with optional fold changes, were entered to evaluate the potential significance of each molecule within the pathway. Topological analysis encompassed assessing impact values by considering degree centrality, which measures the number of links connecting a node; betweenness centrality, which quantifies the number of shortest paths passing through a given node; and closeness centrality, which determines overall distance from a specific node to all others. Enrichment analysis employed the hypergeometric test while topology measure utilized degree centrality, and integration method involved combined queries.

Validation of representative differentially expressed genes in transcriptomics analysis

The 8 representative differential genes were selected to verify the accuracy of transcriptomics data. Corresponding primers for the differential genes were designed through the NCBI website (www.ncbi.nlm.nih.gov), and the primer design results are presented in Table S6. Reverse transcription PCR (RT-PCR) was performed using the HiScript III All-in-one RT SuperMix kit and AceQ qPCR SYBR Green Master Mix kit (Vazyme, Nanjing) based on kit instructions. The reference gene *NAGK* was selected as an internal control for mRNA abundance[34]. Fold changes in the levels of target gene mRNA were determined using the formula $2^{-\Delta\Delta Ct}$. SPSS was used for statistical analysis of sample information and analysis methods such as ANOVA and two independent samples t-test were used for difference analysis. $P < 0.05$ was considered as statistically significant.

Institutional review board statement

This study was granted approval by the Ethics Committee of Henan Children's Hospital (2019-H-K11), and all procedures were conducted in accordance with relevant guidelines and regulations.

Results

The research scheme

The general concept of this research is illustrated in Scheme 1. Metabolomics analysis was conducted on a total of 96 plasma samples, comprising 28 cases of MNA NB and 68 cases of non-MNA NB. Additionally, transcriptomics analysis was performed on 52 tissue samples from NB patients, including 15 cases of MNA NB and 37 cases of non-MNA NB. Ultimately, through the integration and comprehensive analysis of metabolomics and transcriptomics data, we elucidated the aberrant pathway network associated with MNA NB. This study is anticipated to provide a theoretical foundation for investigating the molecular mechanisms underlying MNA NB as well as identifying potential therapeutic targets.

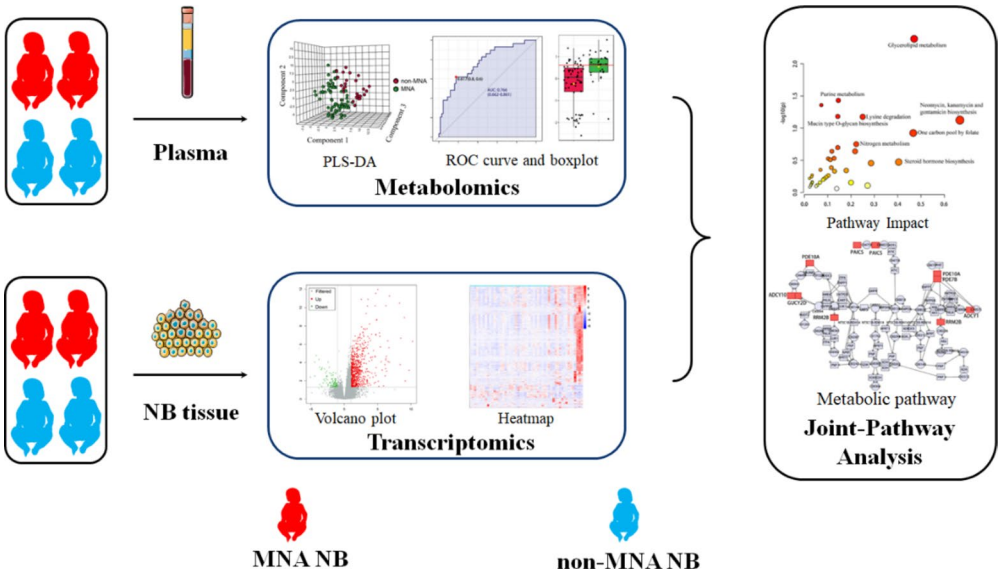

Scheme 1. Schematic diagram of the process of this study.

The Metabolome differences between MNA NB and non-MNA NB

To explore the differences in metabolites between MNA NB and non-MNA NB, plasma metabolomics analysis was first conducted using a non-targeted metabolomics-based approach.

The PCA plot demonstrates the robustness of our results by revealing the close clustering of QC samples under both positive and negative modes (Fig. S2). To visually depict metabolomic differences between MNA NB and non-MNA NB, we performed cluster analysis on plasma metabolites of NB based on compound correlations, which is presented in the form of a heatmap (Fig. S3). The differences between MNA NB and non-MNA NB were visualized using PLS-DA plots in positive mode and negative mode (Fig. 1A and B), while the cross-validation scores plot is presented in Fig. S4. Additionally, volcano plots were employed to illustrate the metabolites in MNA NB and non-MNA NB under positive and negative modes (Fig. 1C and D). Metabolites exhibiting a fold change > 1.2 (fold change < 0.83) with a significance level of $P < 0.05$ in the volcano plot were identified as differential metabolites. In the field of metabolomics, employing positive and negative modes to characterize differentially expressed metabolites can enhance coverage: positive modes effectively capture metabolites with positive charges, such as amino acids and specific peptides; whereas negative modes are suitable for detecting metabolites with negative charges, including certain organic acids and fatty acids. Furthermore, distinct categories of metabolites exhibit varying ionization efficiencies during the process, thus utilizing positive and negative modes separately can enhance the detection sensitivity for specific groups of metabolites. Therefore, a total of 46 metabolites were identified through metabolomics analysis (Table 1). In the positive mode, a total of 28 metabolites in MNA NB exhibited significant alterations, with 13 showing higher expression and 15 showing lower expression. Similarly, in the negative mode, we identified 18 differential compounds specifically associated with MNA NB, comprising of 8 compounds with higher expression and 10 compounds with lower expression. According to the results of differential metabolite analysis, there were significant alterations in the expression of amino acids, carnitine, and esters. These findings suggest that MNA disrupts multiple metabolic classes and may impact the development of MNA NB. Additionally, considering the substantial inter-individual variability in NB, we performed an inter-group comparison heatmap alongside the differential metabolite. Heatmaps depicting the correlation among differential compounds were generated to visually represent the differential metabolites (Fig. 1E and F). In summary, the metabolomics results demonstrate substantial differences in the metabolomics between MNA NB and non-MNA samples.

The altered pathways and biomarkers between MNA NB and non-MNA NB acquired using metabolomics-based approach

The enrichment and pathway analyses were performed on differential metabolites to identify abnormal metabolic pathways between MNA NB and non-MNA NB. Based on the 46 most altered metabolites, significant differences were observed in alpha linolenic acid and linoleic acid metabolism, betaine metabolism, mitochondrial beta-oxidation of short chain saturated fatty acids, methionine metabolism, glycine and serine metabolism in the enrichment analysis (Fig. 2A). In the pathway analysis (Fig. 2B), significant differences were found in glycine, serine and threonine metabolism, biosynthesis of unsaturated fatty acids, and primary bile acid biosynthesis. Furthermore, to investigate the impact of MNA on plasma biomarkers in metabolomics and facilitate subsequent clinical diagnosis, we conducted receiver operating characteristic (ROC) curve analysis for differential metabolites. The expression levels of elaidic carnitine and C16 sphinganine were found to be significantly different between MNA NB and non-MNA NB groups, with all ROC curves exhibiting an area under the curve (AUC) greater than 0.7 (Fig. 2C, D). Additional biomarkers are presented in Fig. S5 and Table S3.

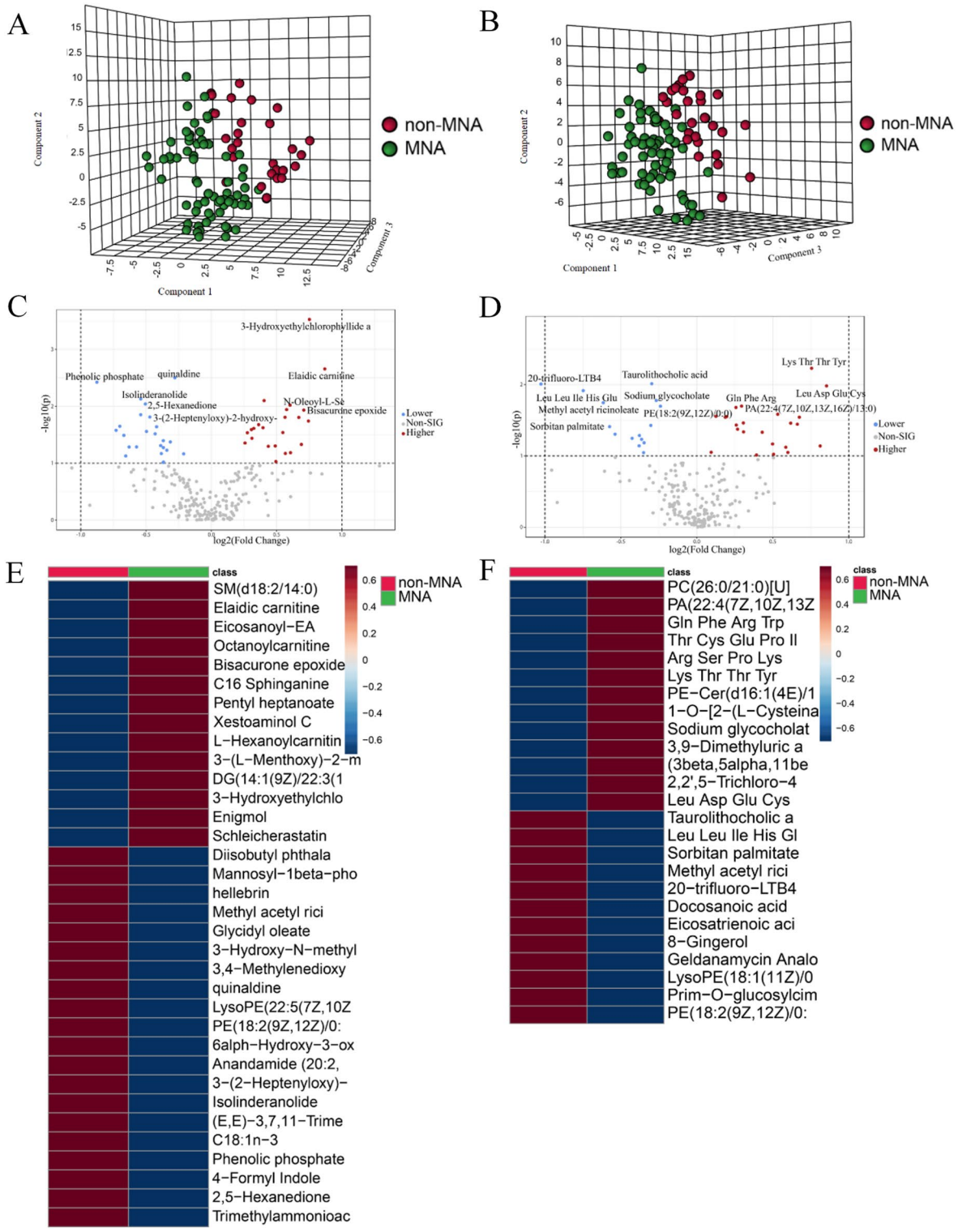

Fig. 1. The plasma metabolomics analysis between MNA NB and non-MNA NB. The PLS-DA results of MNA NB and non-MNA NB in (**A**) positive mode and (**B**) negative mode. The volcano plot of metabolite of MNA NB and non-MNA NB in (**C**) positive mode and (**D**) negative mode. The heatmap shows clear distinction of metabolites between MNA NB and non-MNA NB in (**E**) positive mode and (**F**) negative mode.

Therefore, regulatory metabolic pathways of MNA in NB were identified to include alpha linolenic acid and linoleic acid metabolism, beta oxidation of short chain fatty acids harvested from mitochondria, methyl metabolism, glycine, serine and threonine metabolism, biosynthesis of unsaturated fatty acids, and primary bile acid

NO.	Metabolites	VIP value	Fold change	*P* value	Expression	Mode
1	Phenolic phosphate	2.0419	0.5447	0.004	Lower	Positive
2	(E,E)-3,7,11-Trimethyl-2,6,10-dodecatrienyl heptanoate	1.3231	0.64625	0.052	Lower	Positive
3	Anandamide (20:2, n-6)	1.2881	0.67228	0.052	Lower	Positive
4	Isolinderanolide	1.9276	0.6873	0.007	Lower	Positive
5	Methyl acetyl ricinoleate	1.6441	0.70866	0.028	Lower	Positive
6	Glycidyl oleate	1.8371	0.72134	0.015	Lower	Positive
7	3-(2-Heptenyloxy)-2-hydroxypropyl undecanoate	1.7345	0.74772	0.023	Lower	Positive
8	Diisobutyl phthalate	1.4004	0.76426	0.049	Lower	Positive
9	LysoPE(22:5(7Z,10Z,13Z,16Z,19Z)/0:0)	1.2718	0.76678	0.068	Lower	Positive
10	6α-Hydroxy-3-oxo-5β-cholan-24-oic Acid	1.1805	0.77431	0.097	Lower	Positive
11	Mannosyl-1beta-phosphomy-coketide C30	1.5977	0.77486	0.040	Lower	Positive
12	3,4-Methylenedioxy-benzoic acid	1.3702	0.77529	0.053	Lower	Positive
13	3-Hydroxy-*N*-methylpyridinium	1.3362	0.78963	0.059	Lower	Positive
14	PE(18:2(9Z,12Z)/0:0)	1.4403	0.80419	0.042	Lower	Positive
15	quinaldine	2.3218	0.82394	0.003	Lower	Positive
16	C16 Sphinganine	1.5118	1.2103	0.029	Higher	Positive
17	3-(L-Menthoxy)-2-methylpropane-1,2-diol	1.5552	1.2366	0.026	Higher	Positive
18	Pentyl heptanoate	1.5625	1.3151	0.024	Higher	Positive
19	Eicosanoyl-EA	1.3906	1.4033	0.050	Higher	Positive
20	SM(d18:2/14:0)	1.0469	1.4078	0.093	Higher	Positive
21	DG(14:1(9Z)/22:3(10Z,13Z,16Z)/0:0)[iso2]	1.4438	1.4807	0.067	Higher	Positive
22	L-Hexanoylcarnitinen-butyl ester	1.7871	1.4904	0.011	Higher	Positive
23	*N*-Oleoyl-L-Serine	1.8365	1.5179	0.010	Higher	Positive
24	Schleicherastatin 3	1.1984	1.5215	0.065	Higher	Positive
25	Xestoaminol C	1.4081	1.612	0.047	Higher	Positive
26	Bisacurone epoxide	1.7433	1.6327	0.012	Higher	Positive
27	(±)-Octanoylcarnitine	1.614	1.6736	0.018	Higher	Positive
28	Elaidic carnitine	2.1475	1.825	0.002	Higher	Positive
29	Methyl acetyl ricinoleate	1.9165	0.64537	0.018	Lower	Negative
30	Leu Leu Ile His Glu	2.0268	0.65018	0.025	Lower	Negative
31	Sorbitan palmitate	1.6781	0.6902	0.054	Lower	Negative
32	Docosanoic acid	1.5511	0.74246	0.066	Lower	Negative
33	Prim-*O*-glucosylcimifugin	1.5826	0.75566	0.044	Lower	Negative
34	Eicosatrienoic acid	1.5399	0.78633	0.072	Lower	Negative
35	(±)8-Gingerol	1.6914	0.82259	0.048	Lower	Negative
36	PE(18:2(9Z,12Z)/0:0)	1.883	0.82922	0.013	Lower	Negative
37	Taurolithocholic acid 3-glucuronide	2.0878	0.76077	0.019	Lower	Negative
38	LysoPE(18:1(11Z)/0:0)	1.2226	0.79486	0.091	Lower	Negative
39	Arg Ser Pro Lys	1.6222	1.2435	0.035	Higher	Negative
40	Gln Phe Arg Trp	1.884	1.3103	0.008	Higher	Negative
41	PA(22:4(7Z,10Z,13Z,16Z)/13:0)	1.8049	1.4571	0.020	Higher	Negative
42	(3beta,5alpha,11beta,17beta)-9-Fluoro-17-methyland-rostane-3,11,17-triol	1.7148	1.5435	0.026	Higher	Negative
43	3,9-Dimethyluric acid	1.7036	1.5673	0.030	Higher	Negative
44	PE-Cer(d16:1(4E)/19:0)	1.3171	1.5996	0.057	Higher	Negative
45	Thr Cys Glu Pro Ile	1.7754	1.7976	0.015	Higher	Negative
46	Leu Asp Glu Cys	2.0686	2.1534	0.004	Higher	Negative

Table 1. Differential expressed metabolites between MNA NB and non-MNA NB.

biosynthesis. Additionally, elaidic carnitine and C16 Sphinganine were discovered as potential biomarkers for clinical treatment. In summary, metabolomics revealed multiple abnormal metabolic pathways between MNA NB and non-MNA NB that provide a theoretical basis for investigating the molecular mechanisms underlying MNA NB.

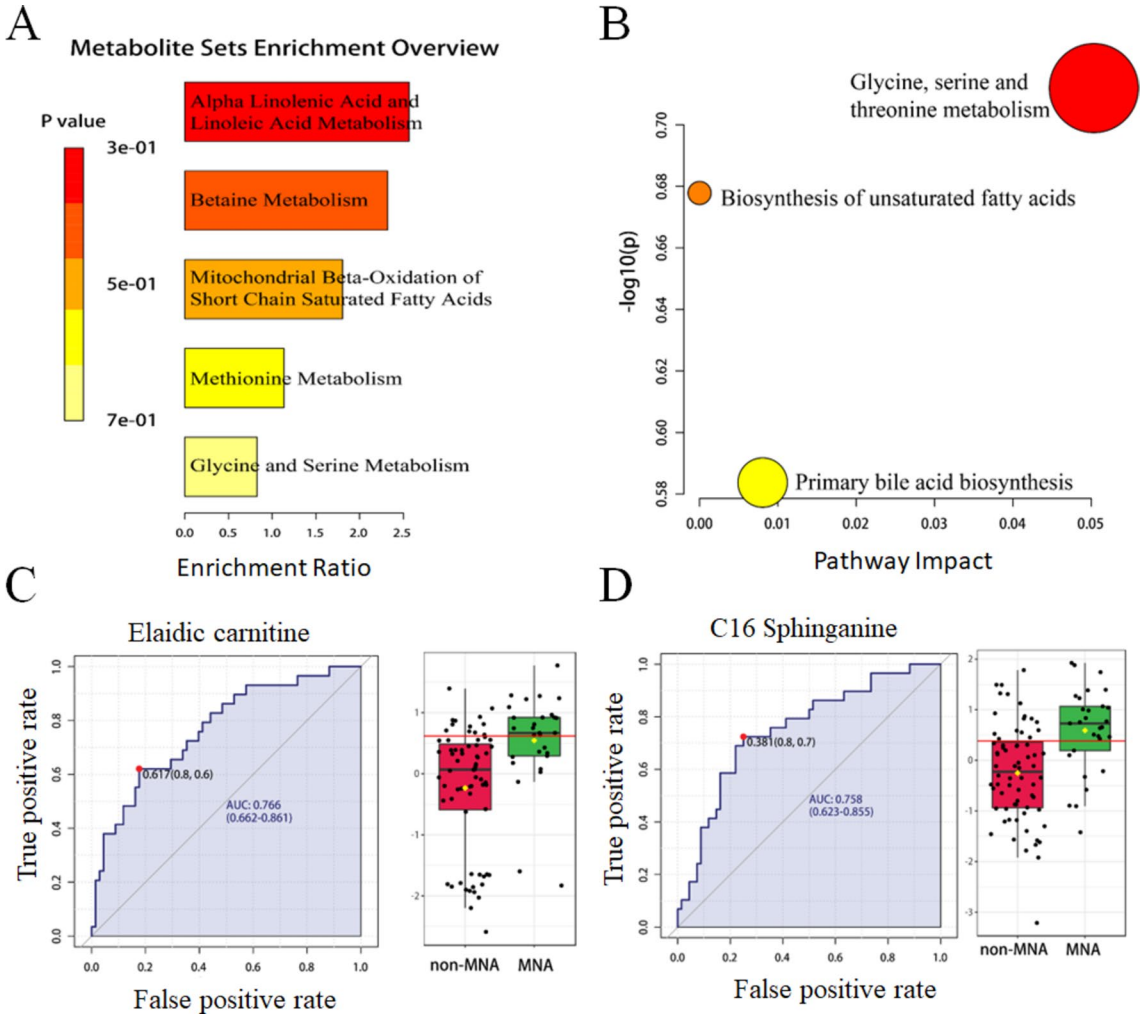

Fig. 2. The altered pathways and biomarkers in metabolomics. (**A**) The enrichment analysis of differential metabolism revealed various metabolic changes between MNA NB and non-MNA NB. (**B**) The pathway analysis revealed significant abnormalities in the pathways between MNA NB and non-MNA NB. The representative metabolic biomarker ROC curve and boxplot of (**C**) elaidic carnitine and (D) C16 Sphinganine.

Transcriptomics analysis uncovers the abnormal expression gene between MNA NB and non-MNA NB

To further investigate the transcriptome differences between MNA NB and non-MNA NB, we conducted a comparative analysis of the transcriptomics from 15 MNA NB tissues and 37 non-MNA NB tissues. The detailed results of RNA quality assessment, including total RNA concentration, A_{260}/A_{280}, A_{260}/A_{230}, 28S/18S ratio, and RIN values for the extracted samples are presented in Table S4. These results confirm that the RNA quality of our NB samples meets the required standards for subsequent analyses. Additionally, preprocessing of sequencing data revealed high-quality raw bases ranging from 6.49G to 7.76G per sample, clean bases ranging from 6.00G to 7.22G per sample, and Q30 base percentages ranging from 92.59 to 95.18% across all samples. Furthermore, the GC content ranged from 44.29 to 50.53%, indicating consistent high data quality among different samples (Table S5). The FPKM values (Fig. S6) and the total number of detected mRNAs in each sample (Fig. S7) reflect the expression abundance of genes across different samples, thereby highlighting inter-sample variations. Moreover, to visually represent the transcriptomics disparities between MNA NB and non-MNA NB, alterations in genes affected by MNA were initially depicted using volcano plots. Differential genes were identified among NB tissue RNAs with $P < 0.05$ and $|\log_2(\text{fold change})| > 1$ in the volcano plot (Fig. 3A). A total of 884 differential genes were discovered, comprising of 766 higher expression genes and 118 lower expression genes (Fig. 3B). The top 20 higher expression and lower expression genes in both MNA and non-MNA NB are presented in Tables 2 and 3 respectively. Furthermore, a cluster analysis heatmap was employed to present the differential gene expression patterns more intuitively (Fig. 3C), demonstrating significant distinctions between MNA NB and non-MNA NB. Based on the transcriptomics results and NB-related literature[35–42], 8 reported differential genes related to NB were selected for RT-PCR validation. These genes included *ALK*, *CIP2A*, *IL10*, *FABP4*, *UNC5D*, *CHL1*, *ERBB3* and *CGA*. RT-PCR results showed that the relative expression levels of *ALK*, *CIP2A*, *IL10* and *FABP4* were higher in MNA NB than in non-MNA NB, while the relative expression levels of *UNC5D*, *CHL1*, *ERBB3* and *CGA*

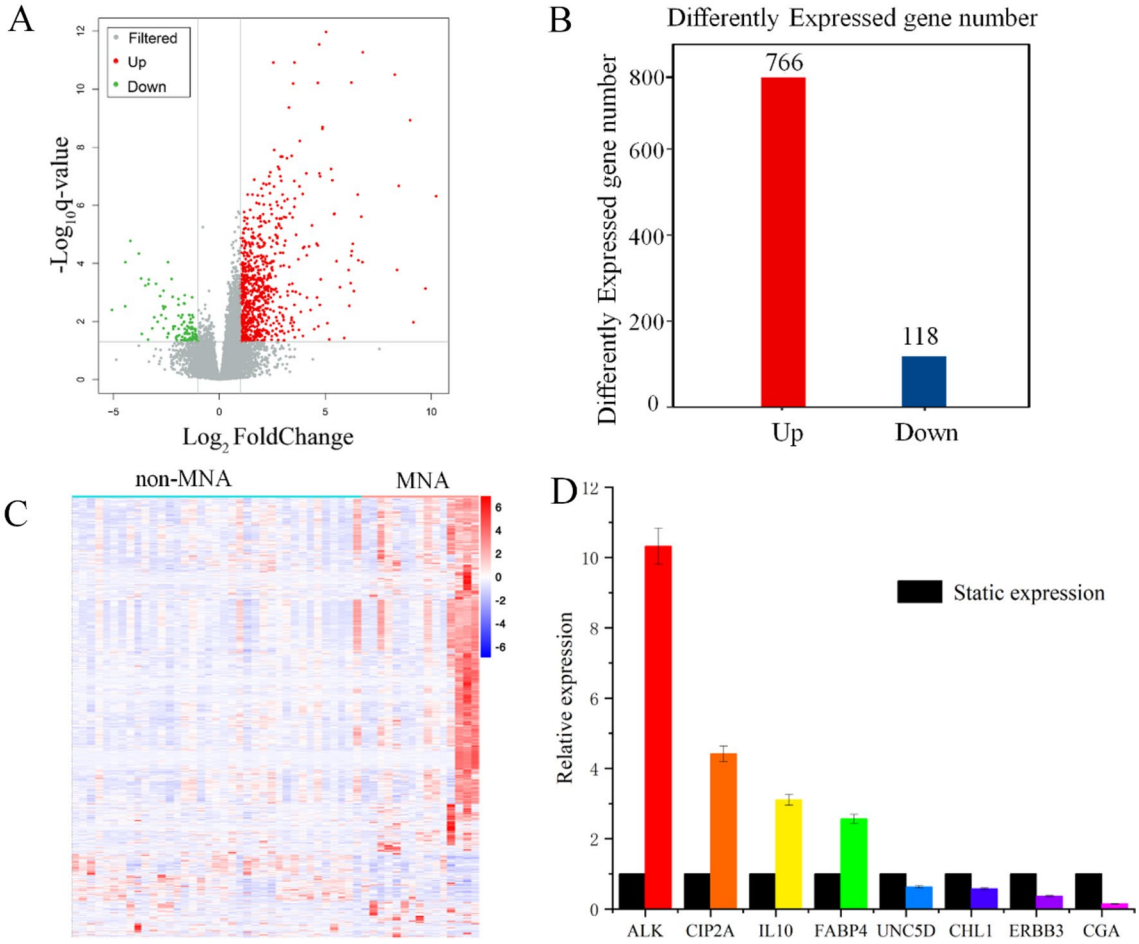

Fig. 3. The NB tissue transcriptomics and validation. (**A**) The volcano plot shows differentially expressed genes between MNA NB and non-MNA NB. (**B**) Number of differentially expressed genes of MNA NB compared to non-MNA NB. (**C**) The heatmap shows segregation of MNA NB and non-MNA NB based on transcriptomics analysis. (**D**) Expression trends of genes in RT-PCR were consistent with transcriptomics results.

were lower in non-MNA NB. In particular, the transcriptomics results were consistent with the RT-PCR results, showing the reliability of the transcriptomics results (Fig. 3D, Table S6). In summary, the transcriptomics results showed that MNA NB and non-MNA NB metabolomes were significantly different.

KEGG and GO analysis between MNA NB and non-MNA NB using transcriptomics-based approach

The differential genes between MNA NB and non-MNA NB were utilized for GO analysis and KEGG analysis to identify aberrant pathways. Metabolic pathways associated with the obtained differential genes were analyzed through GO analysis, aiming to elucidate their potential biological functions (Figs. 4A and S8). Regarding biological processes, the top 3 aberrant expressions consisted of cellular process, single-organism process and biological regulation. Regarding cellular component, the top 3 significantly aberrant expressions were cell, cell part and organelle. Regarding molecular function, the top 3 significantly aberrant expressions were binding, catalytic activity and molecular transducer activity. We further conducted KEGG prediction analysis and observed that the signaling molecules and interaction pathway exhibited the most significant alterations, suggesting an alternative perspective on the biological functions of MNA NB (Figs. 4B, S9). Relationships between differential genes were visualized by protein–protein interaction (PPI) circle diagrams (Fig. S10), illustrating the close connection between genes such as *CDC6*, *CDC45*, *MCM2*, *CCNB1* etc. The identified genes were found to be associated with the processes of mitosis and DNA replication[43], as well as being implicated in abnormalities related to these processes according to the results of GO analysis (Fig. S11). This suggests that MNA may play a pivotal role in the intricate mechanisms governing mitosis and DNA replication. Consequently, cellular process, single-organism process, biological regulation, cell, cell part, organelle, binding, catalytic activity, molecular transducer activity, signaling molecules and interaction were molecular mechanisms of MNA that affected the prognosis of NB. Therefore, based on the transcriptomics method, multiple biological functional differences between MNA NB and non-MNA NB have been discovered, which is expected to provide a theoretical basis for exploring the molecular mechanism of MNA NB.

NO.	Gene	Description	Fold change	*P* value
1	*H4C8*	H4 clustered histone 8	32.563	6.31E−17
2	*H2AC11*	H2A clustered histone 11	28.999	1.43E−12
3	*H3C4*	H3 clustered histone 4	28.915	1.79E−12
4	*H2BC9*	H2B clustered histone 9	26.890	1.67E−10
5	*H4C5*	H4 clustered histone 5	26.245	1.18E−10
6	*H2AC8*	H2A clustered histone 8	26.071	3.39E−16
7	*H2BC18*	H2B clustered histone 18	24.947	2.87E−14
8	*WDR72*	WD repeat domain 72	24.864	2.12E−07
9	*ZNF732*	zinc finger protein 732	20.561	2.69E−08
10	*ABCA12*	ATP binding cassette subfamily A member 12	18.707	2.41E−07
11	*H3C1*	H3 clustered histone 1	17.349	5.77E−07
12	*H4C9*	H4 clustered histone 9	17.067	1.17E−10
13	*H2AC13*	H2A clustered histone 13	15.954	2.54E−07
14	*KCNH5*	potassium voltage-gated channel subfamily H member 5	15.419	2.85E−07
15	*TEX15*	testis expressed 15, meiosis and synapsis associated	15.180	9.92E−10
16	*H2BC11*	H2B clustered histone 11	13.812	5.03E−12
17	*TRIM71*	tripartite motif containing 71	13.666	4.92E−10
18	*PLIN4*	perilipin 4	32.563	8.61E−07
19	*PLIN1*	perilipin 1	28.999	6.80E−08
20	*H3C10*	H3 clustered histone 10	28.915	1.70E−09

Table 2. The top 20 genes significantly higher expression between MNA NB and non-MNA NB.

NO.	Gene	Description	Fold Change	*P* value
1	*CYP11B1*	cytochrome P450 family 11 subfamily B member 1	0.030	< 0.001
2	*HSD3B2*	hydroxy-delta-5-steroid dehydrogenase, 3 beta- and steroid delta-isomerase 2	0.046	< 0.001
3	*GRP*	gastrin releasing peptide	0.046	1.16E−06
4	*NCMAP*	non-compact myelin associated protein	0.054	1.28E−07
5	*CRH*	corticotropin releasing hormone	0.071	4.85E−07
6	*CGA*	glycoprotein hormones, alpha polypeptide	0.077	6.26E−06
7	*GSTA1*	glutathione S-transferase alpha 1	0.079	< 0.001
8	*CYP21A2*	cytochrome P450 family 21 subfamily A member 2	0.088	1.36E−05
9	*CYP17A1*	cytochrome P450 family 17 subfamily A member 1	0.097	0.0047
10	*UCN3*	urocortin 3	0.097	1.15E−05
11	*ADCYAP1*	adenylate cyclase activating polypeptide 1	0.099	7.18E−06
12	*PNPLA5*	patatin like phospholipase domain containing 5	0.111	0.0014
13	*FIBCD1*	fibrinogen C domain containing 1	0.118	< 0.001
14	*SST*	somatostatin	0.125	1.14E−05
15	*SBK2*	SH3 domain binding kinase family member 2	0.132	< 0.001
16	*PROK1*	prokineticin 1	0.143	4.31E−05
17	*SLC25A48*	solute carrier family 25 member 48	0.149	< 0.001
18	*FGF16*	fibroblast growth factor 16	0.157	< 0.001
19	*SFRP5*	secreted frizzled related protein 5	0.160	2.44E−05
20	*LRRC38*	leucine rich repeat containing 38	0.160	0.0013

Table 3. The top 20 genes significantly lower expression between MNA NB and non-MNA NB.

Integrated transcriptomics and metabolomics analyses between MNA NB and non-MNA NB

Multi-omics research employs omics integration, which facilitates the integration of data and regulatory relationships across various levels. This approach enables a comprehensive exploration of the mechanistic actions of specific genes in diseases from diverse perspectives and facets. In order to establish connections between crucial metabolites and genes via shared metabolic pathways, we systematically investigated the altered pathways of MNA in NB and conducted joint-pathway analysis using MetaboAnalyst 5.0. The modified pathways are depicted in

Fig. 4. The GO and KEGG analysis between MNA NB and non-MNA NB in transcriptomics. (**A**) GO analysis of biological processes, molecular functions and cellular components organization between MNA NB and non-MNA NB. (**B**) KEGG analyzes from six aspects of cellular processes, environmental information, genetic information processing, human diseases, metabolism, organismal systems between MNA NB and non-MNA NB.

Fig. 5A and summarized in Table 4, encompassing glycerolipid metabolism, purine metabolism, lysine degradation, as well as other metabolic pathways. These findings suggest that MNA impacts NB through these specific metabolic routes. Glycerolipid metabolism, shown in Fig. 5B, had P values < 0.05 and an impact coefficient of 0.470, and included significantly changed genes consisting of *AGPAT1*, *CEL*, *PLPP4* and *MOGAT3*. As shown in Fig. 5C, in the purine metabolism, the expression levels of *PDE10A*, *PAICS*, *PDE7B*, *ADCY10*, *GUCY2D*, *RRM2B* and *ADCY1* were altered in the MNA NB compared to non-MNA NB. Figure 5D shows that in lysine degradation, *CAMKMT* and *EHMT2* were altered in MNA NB. Abnormal pathways suggest that the molecular mechanism of MNA changes in NB. Related differentially expressed genes by joint-pathway analysis are shown in Table 5 and other altered pathways are shown in Fig. S11, including mucin type O-glycan biosynthesis, nitrogen metabolism, one carbon pool by folate pathway, starch and sucrose metabolism. Hence, glycerolipid metabolism, purine metabolism, and lysine degradation were found to be altered in MNA NB through joint metabolomics and transcriptomics analysis, which could provide a theoretical basis for future treatment of MNA NB.

Discussion

It is well known that the MNA is closely associated with the late stages of NB and poor prognostic outcomes. It has been found that MNA is a potential carcinogenic driver in the developing nervous system and leads to the development of NB[10,44]. However, MNA is not always positively correlated with mRNA or protein expression, suggesting a more complex interaction of MNA with NB[45]. In this study, 96 clinical plasma samples and 52 clinical NB tissue samples were analyzed and 884 differential genes and 46 differential metabolites were identified. Metabolites elaidic carnitine and C16 sphinganine were found to be key metabolites in MNA NB. The metabolomics and transcriptomics characteristics of MNA NB were demonstrated and a comprehensive

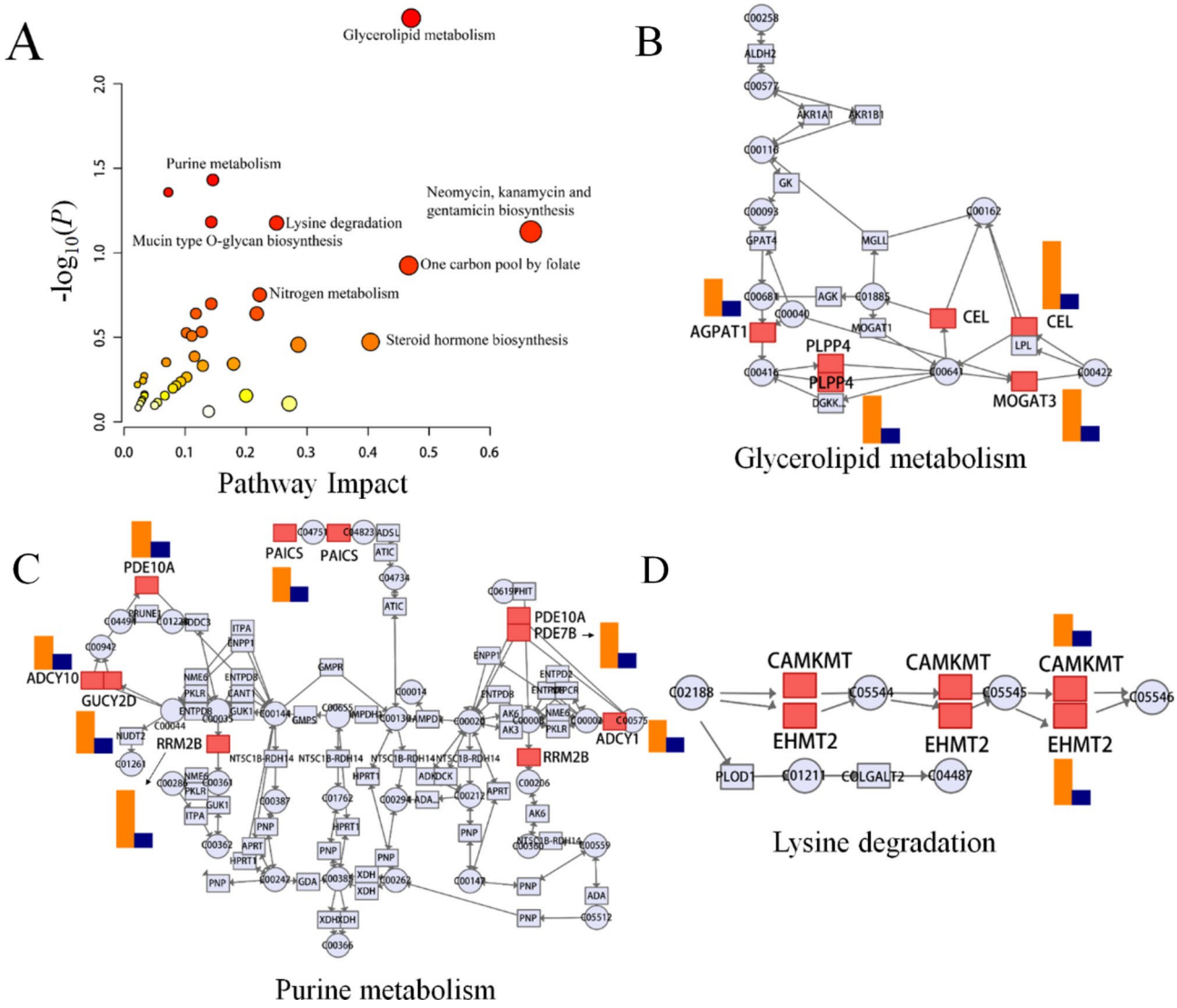

Fig. 5. Integrated transcriptomics and metabolomics analysis of NB metabolic pathways. (**A**) Joint-pathway analysis of differential pathway between MNA NB and non-MNA NB. (**B**) The glycerolipid metabolism pathway, (**C**) the purine metabolism pathway and (**D**) the lysine degradation pathway with altered significantly genes in MNA NB compared to non-MNA NB. (Significant overexpression in red, and no significant changes in grey. The size of the bubbles represents the number of genes enriched, with larger bubbles indicating a higher enrichment level while the color indicates the significance of enrichment, the redder the color, the higher the significance. In (**B**–**D**), the orange color represents the corresponding gene's fold change value, while blue indicates the baseline value.)

NO.	Pathway name	Match status		*P* value	Impact
1	Glycerolipid metabolism	4/35	0.004		0.47059
2	Purine metabolism	7/166	0.037		0.14545
3	Drug metabolism—other enzymes	4/70	0.044		0.072464
4	Mucin type O-glycan biosynthesis	2/22	0.066		0.14286
5	Lysine degradation	3/49	0.067		0.25
6	Neomycin, kanamycin and gentamicin biosynthesis	1/4	0.075		0.66667
7	One carbon pool by folate	2/31	0.119		0.46667
8	Nitrogen metabolism	1/10	0.177		0.22222
9	Starch and sucrose metabolism	2/43	0.200		0.14286
10	Retinol metabolism	2/47	0.229		0.21739

Table 4. Differential metabolic pathways based on joint-pathway analysis.

Gene	Enriched pathway	Function
AGPAT1	Glycerolipid metabolism	1-acylglycerol-3-phosphate *O*-acyltransferase 1
PLPP4	Glycerolipid metabolism	Phospholipid phosphatase 4
CEL	Glycerolipid metabolism	Carboxyl ester lipase
MOGAT3	Glycerolipid metabolism	Monoacylglycerol *O*-acyltransferase 3
PAICS	Purine metabolism	Phosphoribosylaminoimidazole carboxylase and Phosphoribosylaminoimidazo-lesuccinocarboxamide synthase
PDE10A	Purine metabolism	Phosphodiesterase 10A
ADCY10	Purine metabolism	Adenylate cyclase 10
GUCY2D	Purine metabolism	Guanylate cyclase 2D, retinal
PDE7B	Purine metabolism	Phosphodiesterase 7B
RRM2B	Purine metabolism	Ribonucleotide reductase regulatory TP53 inducible subunit M2B
CAMKMT	Lysine degradation	Calmodulin-lysine *N*-methyltransferase
EHMT2	Lysine degradation	Euchromatic histone lysine methyltransferase 2
GALNT8	Mucin type *O*-glycan biosynthesis	Polypeptide *N*-acetylgalactosaminyltransferase 8
CA1	Nitrogen metabolism	Carbonic anhydrase 1
DHFR	One carbon pool by folate	Dihydrofolate reductase
TYMS	One carbon pool by folate	Thymidylate synthetase
HK1	Starch and sucrose metabolism	Hexokinase 1
GYG1	Starch and sucrose metabolism	Glycogenin 1

Table 5. Related differentially expressed genes by joint-pathway analysis.

network analysis was carried out. Compared with non-MNA NB, MNA NB showed significant differences in glycerolipid metabolism, purine metabolism, amino acid metabolism. The genes *GPAT1*, *CEL*, *PLPP4*, *MOGAT3, PDE10A*, *PAICS*, *PDE7B*, *ADCY10*, *GUCY2D*, *RRM2B*, *ADCY1*, *CAMKMT* and *EHMT2* involved in glycerolipid metabolism, purine metabolism, and amino acid metabolism were regulated by MNA. Our study provides deep insight into the molecular mechanism of MNA on NB, and identified key metabolites as potential targets of MNA, providing a basis for future therapeutic research on NB.

MNA affects glycerolipid metabolism in NB

In the joint-pathway analysis, glycerolipid metabolism was found to be significantly changed in MNA NB where *MYCN* can directly regulate glycerolipid synthesis, degradation and accumulation[46]. Additionally, secondary messengers of glycerolipids activate downstream oncogenic signaling and serve as a fatty acid reservoir for energy storage, preventing the accumulation of toxic fatty acids that support tumor growth, corroborating the positive effect of MNA on tumors[47]. Glycerolipid metabolism had been proven to be a potential independent prognostic factor in colon cancer and positively correlated with cancer hallmark pathways including bile acid metabolism, xenobiotic metabolism, and peroxisome and negatively correlated with pathways such as interferon gamma response, allograft rejection, apoptosis, and inflammatory response ($P < 0.05$)[48]. Moreover, the abnormal expression of glycerolipid metabolism in gastric cancer and bladder cancer shows that glycerolipid metabolism plays a key role in tumors[49];[50]. Nevertheless, few studies have reported the changes of glycerolipid metabolism in NB and no research has found the relationship between MNA and glycerolipid metabolism. Therefore, this study raises the question of whether it is possible to improve the prognosis of MNA NB by studying the relationship between MNA and glycerolipid metabolism.

According to the results, there were significant differences in the expression of *AGPAT1*, *CEL*, *PLPP4*, and *MOGAT3* genes. *AGPAT1* has been used as a novel colonic biomarker for discriminating between ulcerative colitis with and without primary sclerosing cholangitis, and abnormalities of *AGPAT1* have also been found between MNA NB and non-MNA NB[51]. Therefore, it is necessary to further study whether *AGPAT1* can also be a therapeutic target of MNA NB. In addition, *MYCN* is also believed to play a key role in promoting fatty acid metabolism for sustainable tumor cell growth, and the cell survival of *MYCN* is also highly dependent on fatty acid uptake, which is consistent with the significant differences in fatty acid metabolism in our metabolomics results, suggesting that fatty acid metabolism may be a promising strategy for HR-NB patients[46]. In conclusion, the discovery of the potential link between glycerolipid metabolism and MNA provides a new perspective for understanding the molecular mechanism of NB.

MNA influenced purine metabolism in NB

The joint-pathway analysis found that purine metabolism was significantly altered in the MNA NB. Purine, as a rich substrate in organism, which includes DNA, RNA, nucleosides and nucleotides, AMP, ADP, ATP, GMP, GDP, GTP, and cyclic forms of cAMP and cGMP, is an important raw material for cell proliferation and an important factor for immune regulation. Purine is involved in the stabilization of immune regulation and the formation of energy carriers and functions, thereby influencing the growth of both cancer and non-cancer

cells[52–54]. Purine metabolism and purine biosynthesis pathway activities were significantly activated in patients with a poor prognosis of hepatocellular carcinoma, and purine metabolism has also been confirmed to change in ovarian cancer, gastric cancer, breast cancer and other cancers[53,55,56]. However, the relationship between MNA and purine metabolism has not yet been reported. This study found that purine metabolism has changed significantly due to MNA. Therefore, we demonstrated that there is a complex relationship between MNA and purine metabolism. Exploring the relationship between MNA and purine, and using purine metabolism to inhibit tumor development is a plausible future research direction. Furthermore, it has been found that *PAICS* knockout in MNA cells significantly reduces cell proliferation, colony formation, migration capacity and DNA synthesis[57]. Chakravarthi et al.[58] found that *PAICS* plays an important role in the proliferation and invasion of prostate cancer cells, identifying it as an effective therapeutic target. Therefore, we also believe that *PAICS* may be an effective therapeutic target for MNA NB. Overall, the change of purine metabolism is of great significance in MNA NB, which lays a foundation for clarifying the molecular mechanism of MNA NB and finding effective therapeutic targets.

MNA affect amino acid metabolism in NB

Through metabolomics and joint-pathway analysis, our results showed that amino acid metabolism changed dramatically in MNA NB. In metabolomics, we found significant differences in glycine, serine and threonine metabolism. Serine-glycine metabolism has been found to be critical for tumorigenesis[59,60]. On the other hand, serine and glycine are synthesized from glycolysis through oxidation of the intermediate 3-PGA, which consists of two processes: de novo serine synthesis from glucose and reversible interconversion of serine into glycine[61]. These products fuel one-carbon metabolism. In addition, Xia et al.[62] found that NB cells with MNA show increased transcriptional activation of the serine-glycine-one-carbon biosynthetic pathway and an increased dependence on this pathway for supplying glucose-derived carbon for serine and glycine synthesis. Metabolic abnormalities of serine and glycine were also observed in other cancers, such as glioblastoma and non-small cell lung cancer[63,64]. In the joint-pathway analysis, we found that lysine degradation was a significantly changed pathway. Lysine is an essential amino acid for the human body, and it must be taken in sufficient amount to maintain protein synthesis. It has been found that the lysine degradation pathway is clinically relevant due to the occurrence of two severe neurometabolic disorders (pyridoxine-dependent epilepsy and glutaric aciduria type 1)[65]. In addition, lysine degradation may also be related to the development of early myocardial hypertrophy[66]. Moreover, lysine degradation was found to be significantly different between MNA NB and non-MNA NB, and the potential mechanism of lysine degradation in MNA NB requires further study. Overall, this study showed that amino acid metabolism plays a significant role in the initiation and progression of MNA NB, and the disclosure of amino acid metabolism is expected to offer novel opportunities for advancing the treatment and prognostic evaluation of NB.

Potential therapeutic targets of MNA NB

The discovery of effective therapeutic targets of MNA NB is very important for improving the therapeutic effect of MNA NB. The study conducted by Schonheer et al.[67] demonstrated that both wild-type and acquired *ALK* mutants can induce the transcription of the *MYCN* promoter through the activation of the downstream molecule *ERK*, thereby activating *MYCN* mRNA transcription in neurons and NB. The *ALK* gene is a direct transcriptional target of *MYCN*, and *MYCN*-induced *ALK* activation contributed to the occurrence and development of NB[68–70]. Hasan et al., discovered that *MYCN* has a positive feedback loop which directly regulates *ALK* expression, thereby enhancing *MYCN*'s oncogenic activity and promoting rapid malignant transformation. Additionally, overexpression of *MYCN* induces promoter activity of the *ALK* gene, resulting in elevated levels of *ALK* expression in NB cells[71]. The present study further substantiates the significant upregulation of *ALK* in MNA NB tissues, thereby reinforcing the strong correlation between *ALK* and MNA. In human cancer cells, *CDK2* is an essential component of the cell cycle with key function in tumorigenesis[72]. Our findings also confirmed the relationship between *CDK2* and MNA, thus further investigation into the underlying mechanism between *CDK2* and MNA may help promote a new treatment strategy for MNA NB[73]. Nozato et al.[74] found that the expression level of *ERBB3* was significantly reduced in MNA NB, confirming that the low expression of *ERBB3* affected the progression of NB by affecting the mechanism of epithelial-mesenchymal transition. The decreased expression of *ERBB3* was also associated with MNA NB and poor survival rate. The transcriptomics and RT-PCR findings in our study further support the notion of diminished *ERBB3* gene expression in MNA NB, thus reinforcing the established association between *ERBB3* and MNA. Therefore, these genes should be further studied as potential therapeutic targets to improve the prognosis of MNA NB.

According to the results presented in Table 2, our findings indicate that the significantly altered differentially expressed genes primarily pertain to histones, which are fundamental components of chromatin organization. Histones form a protein complex around which DNA is wrapped, forming nucleosomes. These histone proteins can undergo specific amino acid residue modifications such as acetylation or methylation, and these modifications play a crucial role in regulating gene expression[75]. The regulation of gene expression through the remodeling of tryptophan structure is governed by histone deacetylases, a class of enzymes. However, dysregulation in the expression and activity of these enzymes leads to an imbalance in histone acetylation, thereby promoting the progression of NB[76].

Based on our KEGG results, we have identified the significant involvement of the immune system in NB. The immune evasion of NB is facilitated by various mechanisms, including low immunogenicity, upregulation of immune checkpoint molecules, and secretion of immunomodulatory mediators. These characteristics make it a unique model for studying tumor immunity. Currently, it is widely accepted that the diminished immunogenicity in NB can be attributed to MNA, which leads to reduced expression of MHC-I in HR-NB patients compared to

those with LR-NB. This poses a significant challenge for T cell-mediated immunotherapy[77]. On the contrary, NB cells secrete transforming growth factor β1 and galectin-1, which induce functional impairment in cytotoxic T lymphocytes and NK cells, consequently leading to immunosuppression[78].

Based on joint analysis, we have identified a correlation between drug metabolism enzymes and aberrant biosynthesis of neomycin, kanamycin, and gentamicin. However, it is important to note that these antibiotics are not utilized in the clinical management of NB; therefore, further investigation is required to establish any specific potential association.

Conclusion

In summary, a metabolomic-based approach identified 46 differential metabolites between MNA NB and non-MNA NB. Enrichment analysis revealed significant differences in the metabolism of alpha linolenic acid, linoleic acid, and betaine. Transcriptomics analysis further identified 884 differential genes between MNA NB and non-MNA NB. GO analysis demonstrated significant alterations in biological functions such as cellular processes, single organizational processes, and biological regulations when comparing MNA NB to non-MNA NB. In addition, the KEGG analysis revealed significant alterations in signaling molecules and interactions between MNA NB and non-MNA NB. Specifically, the joint-pathway analysis demonstrated notable disparities in the expression of glycerolipid metabolism, purine metabolism, and lysine degradation pathways between MNA-NB and non-MNA NB, suggesting that MNA impacts glycerolipid metabolism, purine metabolism, and amino acid metabolism in NB. Furthermore, ALK and CDK2 were identified as potential therapeutic targets for MNA NB. In conclusion, this study provides a theoretical foundation for investigating the molecular mechanisms underlying MNA NB and identifying potential therapeutic targets.

Data availability

We have submitted the raw RNA-seq data to NCBI (https://www.ncbi.nlm.nih.gov/sra) under the accession number PRJNA884866. Besides, we have uploaded mass spectrometry data to the MetaboLights (https://www.ebi.ac.uk/metabolights/) with the number of MTBLS6352.

Received: 8 January 2024; Accepted: 26 August 2024
Published online: 30 August 2024

References

1. Beaudry, P. *et al.* A pilot study on the utility of serum metabolomics in neuroblastoma patients and xenograft models. *Pediatr. Blood Cancer* **63**, 214–220 (2016).
2. Zhou, X. *et al.* Therapy resistance in neuroblastoma: Mechanisms and reversal strategies. *Front. Pharmacol.* **14**, 1114295 (2023).
3. Liu, J. *et al.* Perioperative hypertension and anesthetic management in patients undergoing resection of neuroblastoma. *Paediatr. Anaesth.* **33**, 577–582 (2023).
4. Lundberg, K. I., Treis, D. & Johnsen, J. I. Neuroblastoma heterogeneity, plasticity, and emerging therapies. *Curr. Oncol. Rep.* **24**, 1053–1062 (2022).
5. Zhang, H. *et al.* A Mycn-independent mechanism mediating secretome reprogramming and metastasis in Mycn-amplified neuroblastoma. *Sci. Adv.* **9**, eadg6693 (2023).
6. Irwin, M. S. *et al.* Revised neuroblastoma risk classification system: A report from the children's oncology group. *J. Clin. Oncol.* **39**, 3229–3241 (2021).
7. Lee, J. W. *et al.* Clinical significance of Mycn amplification in patients with high-risk neuroblastoma. *Pediatr. Blood Cancer.* **65**, e27257 (2018).
8. Chui, C. Effects of preoperative chemotherapy on neuroblastoma with Mycn amplification: A surgeon's perspective. *World J. Pediatr. Surg.* **3**, e000129 (2020).
9. Rickman, D. S., Schulte, J. H. & Eilers, M. The expanding world of N-Myc–driven tumors. *Cancer Discov.* **8**, 150–163 (2018).
10. Otte, J., Dyberg, C., Pepich, A. & Johnsen, J. I. Mycn function in neuroblastoma development. *Front. Oncol.* **10**, 624079 (2021).
11. Chen, L. *et al.* P53 is a direct transcriptional target of Mycn in neuroblastoma. *Cancer Res.* **70**, 1377–1388 (2010).
12. Ren, P. *et al.* Atf4 and N-Myc coordinate glutamine metabolism in Mycn-amplified neuroblastoma cells through Asct2 activation. *J. Pathol.* **235**, 90–100 (2015).
13. Oliynyk, G. *et al.* Mycn-enhanced oxidative and glycolytic metabolism reveals vulnerabilities for targeting neuroblastoma. *Iscience* **21**, 188–204 (2019).
14. Tjaden, B. *et al.* N-Myc-induced metabolic rewiring creates novel therapeutic vulnerabilities in neuroblastoma. *Sci. Rep.* **10**, 7157 (2020).
15. Floros, K. V. *et al.* Mycn upregulates the transsulfuration pathway to suppress the ferroptotic vulnerability in Mycn-amplified neuroblastoma. *Cell Stress* **6**, 21–29 (2022).
16. Arlt, B. *et al.* Inhibiting phosphoglycerate dehydrogenase counteracts chemotherapeutic efficacy against Mycn-amplified neuroblastoma. *Int. J. Cancer* **148**, 1219–1232 (2021).
17. Alptekin, A. *et al.* Glycine decarboxylase is a transcriptional target of Mycn required for neuroblastoma cell proliferation and tumorigenicity. *Oncogene* **38**, 7504–7520 (2019).
18. Costa, V., Angelini, C., De Feis, I. & Ciccodicola, A. Uncovering the complexity of transcriptomes with Rna-Seq. *J. Biomed. Biotechnol.* **2010**, 1–19 (2010).
19. Du, B. *et al.* Joint analysis of the metabolomics and transcriptomics uncovers the dysregulated network and develops the diagnostic model of high-risk neuroblastoma. *Sci. Rep.* **13**, 16991 (2023).
20. Fan, X. *et al.* A comprehensive analysis of potential prognostic biomarkers for Mycn-amplified neuroblastoma. *Zhongguo Dang Dai Er Ke Za Zhi.* **22**, 262–268 (2020).
21. Lee, E. *et al.* Genomic profile of Mycn non-amplified neuroblastoma and potential for immunotherapeutic strategies in neuroblastoma. *BMC Med. Genom.* **13**, 171 (2020).
22. Shinno, Y. *et al.* Polycomb Ezh1 regulates cell Cycle/5-fluorouracil sensitivity of neuroblastoma cells in concert with Mycn. *Cancer Sci.* **113**, 4193–4206 (2022).
23. Spyropoulos, F. *et al.* Metabolomic and transcriptomic signatures of chemogenetic heart failure. *Am. J. Physiol. Heart Circul. Physiol.* **322**, H451–H465 (2022).
24. Zhao, P. *et al.* Integration of transcriptomics and metabolomics reveals the antitumor mechanism underlying tadalafil in colorectal cancer. *Front. Pharmacol.* **13**, 793499 (2022).

25. Loras, A. *et al.* Integrative metabolomic and transcriptomic analysis for the study of bladder cancer. *Cancers* **11**, 686 (2019).
26. Cavill, R., Jennen, D., Kleinjans, J. & Briedé, J. J. Transcriptomic and metabolomic data integration. *Brief. Bioinform.* **17**, 891–901 (2016).
27. Bolger, A. M., Lohse, M. & Usadel, B. Trimmomatic: A flexible trimmer for illumina sequence data. *Bioinformatics* **30**, 2114–2120 (2014).
28. Kim, D., Langmead, B. & Salzberg, S. L. Hisat: A fast spliced aligner with low memory requirements. *Nat. Methods* **12**, 357–360 (2015).
29. Roberts, A., Trapnell, C., Donaghey, J., Rinn, J. L. & Pachter, L. Improving Rna-Seq expression estimates by correcting for fragment bias. *Genome Biol.* **12**, R22 (2011).
30. Trapnell, C. *et al.* Transcript assembly and quantification by Rna-Seq reveals unannotated transcripts and isoform switching during cell differentiation. *Nat. Biotechnol.* **28**, 511–515 (2010).
31. Kanehisa, M. Kegg: Kyoto encyclopedia of genes and genomes. *Nucleic. Acids. Res.* **28**, 27–30 (2000).
32. Kanehisa, M. Toward understanding the origin and evolution of cellular organisms. *Protein Sci.* **28**, 1947–1951 (2019).
33. Kanehisa, M., Furumichi, M., Sato, Y., Kawashima, M. & Ishiguro-Watanabe, M. KEGG for taxonomy-based analysis of pathways and genomes. *Nucleic Acids Res.* **51**, D587–D592 (2023).
34. Liang, Y. *et al.* Dual isothermal amplification all-in-one approach for rapid and highly sensitive quantification of plasma circulating Mycn gene of neuroblastoma. *Anal. Biochem.* **658**, 114922 (2022).
35. O'Donohue, T. *et al.* Differential impact of Alk mutations in neuroblastoma. *Jco Precis. Oncol.* **5**, 492–500 (2021).
36. Bo, L. *et al.* Bioinformatics analysis of the Cdk2 functions in neuroblastoma. *Mol. Med. Rep.* **17**, 3951–3959 (2018).
37. Urso, C. J. & Zhou, H. Role of Cd36 in palmitic acid lipotoxicity in Neuro-2a neuroblastoma cells. *Biomolecules* **11**, 1567 (2021).
38. Zhen, Z. *et al.* Involvement of Il-10 and Tgf-B in Hla-E-mediated neuroblastoma migration and invasion. *Oncotarget* **7**, 44340–44349 (2016).
39. Miao, L. *et al.* Fabp4 deactivates Nf-Kb-Il1A pathway by ubiquitinating atpb in tumor-associated macrophages and promotes neuroblastoma progression. *Clin. Transl. Med.* **11**, e395 (2021).
40. Wang, H. *et al.* Unc5D regulates P53-dependent apoptosis in neuroblastoma cells. *Mol. Med. Rep.* **9**, 2411–2416 (2014).
41. Ognibene, M. *et al.* Chl1 gene acts as a tumor suppressor in human neuroblastoma. *Oncotarget* **9**, 25903–25921 (2018).
42. Wilzen, A. *et al.* Erbb3 is a marker of a ganglioneuroblastoma/ganglioneuroma-like expression profile in neuroblastic tumours. *Mol. Cancer.* **12**, 70 (2013).
43. He, Y. *et al.* Integrated transcriptome analysis reveals the impact of photodynamic therapy on cerebrovascular endothelial cells. *Front. Oncol.* **11**, 731414 (2021).
44. Swartling, F. J. *et al.* Distinct neural stem cell populations give rise to disparate brain tumors in response to N-Myc. *Cancer Cell.* **21**, 601–613 (2012).
45. Eberherr, C. *et al.* Targeting excessive Mycn expression using Mln8237 and Jq1 impairs the growth of hepatoblastoma cells. *Int. J. Oncol.* **54**, 1853–1863 (2019).
46. Tao, L. *et al.* Mycn-driven fatty acid uptake is a metabolic vulnerability in neuroblastoma. *Nat. Commun.* **13**, 3728 (2022).
47. Ackerman, D. *et al.* Triglycerides promote lipid homeostasis during hypoxic stress by balancing fatty acid saturation. *Cell Rep.* **24**, 2596–2605 (2018).
48. Wang, Z. *et al.* Multi-omics characterization of a glycerolipid metabolism-related gene enrichment score in colon cancer. *Front. Oncol.* **12**, 881953 (2022).
49. Xiong, Z. *et al.* Exploration of lipid metabolism in gastric cancer: A novel prognostic genes expression profile. *Front. Oncol.* **11**, 712746 (2021).
50. Chen, P., Chen, J., He, L., Du, C. & Wang, X. Identification of Circrna-Mirna-Mrna regulatory network in bladder cancer by integrated analysis. *Urol. Int.* **105**, 705–715 (2021).
51. Vessby, J. *et al.* Agpat1 as a novel colonic biomarker for discriminating between ulcerative colitis with and without primary sclerosing cholangitis. *Clin. Transl. Gastroenterol.* **13**, e00486 (2022).
52. La Grotta, R. *et al.* Anti-inflammatory effect of Sglt-2 inhibitors via uric acid and insulin. *Cell. Mol. Life Sci.* **79**, 273 (2022).
53. Liu, J. *et al.* Targeting purine metabolism in ovarian cancer. *J. Ovarian Res.* **15**, 1–93 (2022).
54. De Vitto, H., Arachchige, D., Richardson, B. & French, J. The intersection of purine and mitochondrial metabolism in cancer. *Cells* **10**, 2603 (2021).
55. Syniachenko, O. V., Aliiev, R. F., Iermolaieva, M. V. & Bondar, V. G. The changes in purine metabolism in gastric cancer. *Gastroenterology* **53**, 223–229 (2019).
56. Chen, X. & Chen, J. Mir-10B-5P-mediated upregulation of Piezo1 predicts poor prognosis and links to purine metabolism in breast cancer. *Genomics.* **114**, 110351 (2022).
57. Cheung, C. H. Y. *et al.* "Abstracts of the 77Th Annual Meeting of the Japanese Cancer Association; 2018 Sept 27–29; Osaka, Japan" as Cancer Science, Supplement 2, Vol 109 (2018). *Cancer Sci.* **109**(Suppl 2), 1–1444 (2018).
58. Chakravarthi, B. V. S. K. *et al.* Expression and role of Paics, a De Novo purine biosynthetic gene in prostate cancer. *The Prostate* **77**, 10–21 (2017).
59. Ding, J. *et al.* The histone H3 methyltransferase G9a epigenetically activates the serine-glycine synthesis pathway to sustain cancer cell survival and proliferation. *Cell Metab.* **18**, 896–907 (2013).
60. Zhao, E. *et al.* Kdm4C and Atf4 cooperate in transcriptional control of amino acid metabolism. *Cell Rep.* **14**, 506–519 (2016).
61. Zhao, E., Hou, J. & Cui, H. Serine-glycine-one-carbon metabolism: Vulnerabilities in Mycn-amplified neuroblastoma. *Oncogenesis N. Y. N. Y.* **9**, 14 (2020).
62. Xia, Y. *et al.* Metabolic reprogramming by Mycn confers dependence on the serine-glycine-one-carbon biosynthetic pathway. *Cancer Res.* **79**, 3837–3850 (2019).
63. Liao, L. *et al.* Upregulation of phosphoserine phosphatase contributes to tumor progression and predicts poor prognosis in non-small cell lung cancer patients. *Thorac. Cancer* **10**, 1203–1212 (2019).
64. Kim, D. *et al.* Shmt2 drives glioma cell survival in ischaemia but imposes a dependence on glycine clearance. *Nature* **520**, 363–367 (2015).
65. Leandro, J. & Houten, S. M. The lysine degradation pathway: Subcellular compartmentalization and enzyme deficiencies. *Mol. Genet. Metab.* **131**, 14–22 (2020).
66. Liu, J., Hu, J., Tan, L., Zhou, Q. & Wu, X. Abnormalities in lysine degradation are involved in early cardiomyocyte hypertrophy development in pressure-overloaded rats. *BMC Cardiovasc. Disord.* **21**, 403 (2021).
67. Schönherr, C. *et al.* Anaplastic lymphoma kinase (Alk) regulates initiation of transcription of Mycn in neuroblastoma cells. *Oncogene* **31**, 5193–5200 (2012).
68. Htike, W., Islam, M. A., Hasan, M. T., Ferdous, S. & Rifat, M. Factors associated with treatment delay among tuberculosis patients referred from a tertiary hospital in Dhaka City: A cross-sectional study. *Public Health Action* **3**, 317–322 (2013).
69. Kramer, M., Ribeiro, D., Arsenian-Henriksson, M., Deller, T. & Rohrer, H. Proliferation and survival of embryonic sympathetic neuroblasts by Mycn and activated Alk signaling. *J. Neurosci.* **36**, 10425–10439 (2016).
70. Schönherr, C. *et al.* Anaplastic lymphoma kinase (Alk) regulates initiation of transcription of Mycn in neuroblastoma cells. *Oncogene.* **31**, 5193–5200 (2012).
71. Hasan, M. K. *et al.* Alk is a Mycn target gene and regulates cell migration and invasion in neuroblastoma. *Sci. Rep.* **3**, 3450 (2013).

72. Liang, X. H. *et al.* Mapre1 promotes cell cycle progression of hepatocellular carcinoma cells by interacting with Cdk2. *Cell Biol. Int.* **44**, 2326–2333 (2020).
73. Gogolin, S. *et al.* Cdk4 inhibition restores G1-S arrest in Mycn-amplified neuroblastoma cells in the context of doxorubicin-induced Dna damage. *Cell Cycle* **12**, 1091–1104 (2014).
74. Nozato, M., Kaneko, S., Nakagawara, A. & Komuro, H. Epithelial-mesenchymal transition-related gene expression as a new prognostic marker for neuroblastoma. *Int. J. Oncol.* **42**, 134–140 (2013).
75. DuBois, S. G. & Park, J. R. Neuroblastoma and histone demethylation. *N. Engl. J. Med.* **379**, 1476–1477 (2018).
76. Phimmachanh, M., Han, J. Z. R., Donnell, Y. E. I., Latham, S. L. & Croucher, D. R. Histone deacetylases and histone deacetylase inhibitors in neuroblastoma. *Front. Cell. Dev. Biol.* **8**, 578770 (2020).
77. Aiken, T. J. *et al.* Mechanism of effective combination radio-immunotherapy against 9464D-Gd2, an immunologically cold murine neuroblastoma. *J. Immunother. Cancer* **10**, e004834 (2022).
78. Wienke, J. *et al.* The immune landscape of neuroblastoma: Challenges and opportunities for novel therapeutic strategies in pediatric oncology. *Eur. J. Cancer* **144**, 123–150 (2021).

Acknowledgements
The authors sincerely thank all participants for participating in this study, as this study would not be possible without their valuable contributions.

Author contributions
The manuscript was written by B. D.; Y. Z. and P. Z. collected the data; M. Z., Z. Y., L. L. and L. H. analyzed the data; Q. W. organized the charts. X. Z. were responsible for the experimental design, while W. Z. oversaw the overall study. All authors critically reviewed the manuscript.

Funding
This work were funded by National Natural Science Foundation of China (32201237), Scientific and technological projects of Henan province (222102310270, 222102310109, 232102311135), Henan medical science and technology program (LHGJ20220767), Henan International Joint Laboratory for Prevention and Treatment of Pediatric Disease foundation (EKB202204).

Competing interests
The authors declare no competing interests.

Informed consent
Informed consent was signed by children or their parents.

Additional information
Supplementary Information The online version contains supplementary material available at https://doi.org/10.1038/s41598-024-71211-x.

Correspondence and requests for materials should be addressed to Q.W., X.Z. or W.Z.